On the Analysis of a Transition to a Layered Ridged Dielectric Waveguide

A. G. Engel, Jr. and Linda P. B. Katehi

Electrical Engineering and Computer Science Department
The University of Michigan
Ann Arbor MI 48109-2122

Abstract **— In sub-mm and THz monolithic circuits, transitions between layered ridged dielectric waveguides and power sources may include short lengths of conductor. An integral equation-mode matching technique is expanded so that such a transition may be analyzed, and results for one-port discontinuities in microstrip on a dielectric ridge and preliminary characterization of an actual transition are presented.**

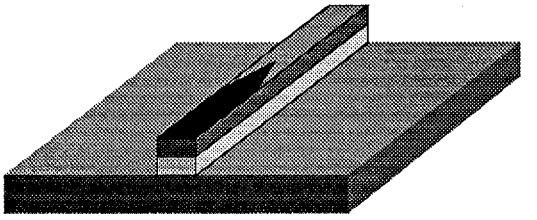

Figure 1: Example of a transition to a ridged dielectric waveguide.

I. INTRODUCTION

The excessive ohmic losses of microstrip in the sub-mm and THz frequency ranges force the monolithic circuit designer to seek out new means for power propagation. One promising candidate for such a transmission line is layered ridged dielectric waveguide [1]. This type of waveguide consists of a dielectric ridge on a substrate, and the ridge consists of two or more layers. Proper choice of dielectric constant in each layer enables the power to be confined in a single, low-loss layer. These waveguides are constructed from dielectric materials and structures which are available in monolithic technology so that the use of the waveguides in integrated circuits is possible.

When these waveguides are integrated with sources of power (such as active devices), or when these waveguides are used to form passive circuit components (such as a power combiner), short lengths of conductor may be used to minimize radiation. For example, a transition between a power source and a dielectric waveguide would have the configuration displayed in Figure 1. The ridge is shown with two layers, and the conductor on the top of the ridge is tapered to minimize unwanted reflections. Due to the high operating frequencies of these structures, accurate characterization can only be accomplished with full-wave analysis techniques.

The presence of the ridge in Figure 1 suggests that the transition be modeled by means of a hybrid method which combines well-known integral equation and mode matching techniques. In its initial presentation in 1991 [2], the integral equation-mode matching (IEMM) technique was applied to the relatively simple two-dimensional configuration of coupled microstrip on dielectric ridges with no substrate. The IEMM technique is sufficiently versatile so that it may be extended in a straightforward manner to three-dimensional structures such as a transition.

In this paper, the three-dimensional IEMM technique is presented, with emphasis on the extensions of the technique from 2D to 3D problems and from simple microstrip on ridges to more complicated multi-layered structures. The analysis of some simple geometries is presented as evidence of the utility of the numerical technique. Finally, preliminary results and future considerations which are necessary for the full characterization of a transition are discussed.

II. THEORY

The structure which is to be analyzed is shown in Figure 2. The outer walls are perfect electric conductors. Along the y-axis, the structure is divided into four sections at $y = b_1, b_2, b_3$. Sections A and D consist of one layer each, and sections B and C are divided into three layers along the x-axis at $x = a_1, a_2$. A conducting strip is located parallel to the x-axis at $y = b_3$. The y-dimension of the strip is assumed to be negligible. The cavity extends from $z = 0$ to $z = c$ and, except for the conducting strip, the cavity is uniform in the z-direction. The integral equation-mode matching technique may be used to evaluate a structure which has an arbitrary number of conductors parallel to the x-axis and an arbitrary number of sections with each section having an arbitrary number of layers, but, for simplicity and brevity, only the theory for the specific structure of interest is considered here.

The discontinuity is characterized from the currents on the conducting strip, which are determined by solving Pocklington's integral equation in the spatial domain. The

IF2

CH3141-9/92/0000-0983$01.00 © 1992 IEEE

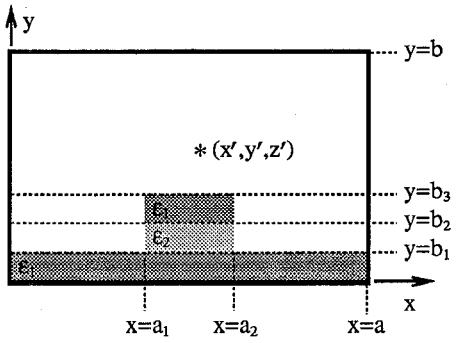

Figure 2: Cross-section of the structure to be analyzed; the conducting strip has been replaced by point source at (x', y', z').

integral equation may be written as

$$\bar{E} = \int_{S'} \overline{\overline{G}}_E \cdot \bar{J}\, dS' \qquad (1)$$

where $\overline{\overline{G}}_E$ is the dyadic electric field Green's function associated with the structure, $\bar{J}$ is the surface current on the conducting strip, and S' represents the surface of the conducting strip. The Green's function is the electric field when the conducting strip is replaced with a current source at (x', y', z').

The Green's function is derived by considering each section of the structure as a section of inhomogeneous parallel plate waveguide. In each section, the fields consist of infinite sums of TE_x and TM_x modes. Away from the source, the fields satisfy the homogeneous wave equation, and may be determined using vector potentials $\bar{A} = a_x(x,y,z)\hat{x}$ and $\bar{F} = f_x(x,y,z)\hat{x}$ via

$$\bar{E} = -j\omega\bar{A} + \frac{1}{j\omega\epsilon\mu}\nabla\nabla\cdot\bar{A} + \frac{1}{\epsilon}\nabla\times\bar{F} \qquad (2)$$

$$\bar{H} = \frac{1}{\mu}\nabla\times\bar{A} + j\omega\bar{F} - \frac{1}{j\omega\epsilon\mu}\nabla\nabla\cdot\bar{F} \qquad (3)$$

The x-, y- and z-dependencies of a_x and f_x are separable. From the uniformity of the cavity in the z-direction and the boundary conditions at $z = 0, c$, the z-dependence in all sections is deduced to be $\cos k_z(z-c)$ for the TE_x modes and $\sin k_z(z-c)$ for the TM_x modes, where $k_z = n\pi/c$.

The boundary conditions at each layer interface and at the upper and lower conducting walls determine the x-dependence of the fields in each layer in a given section [3]. Specifically, these boundary conditions are used to generate transcendental equations for the x-directed wavenumbers and expressions for the unknown constants associated with the x-dependence.

The y-dependence Y of the fields consists of infinite sums of plane waves. In sections A, B, and C, the y-dependencies are of the form

$$Y^A \sim \sum_{l,n}\left(A^+_{ln}e^{-jk_{yln}y} \pm A^-_{ln}e^{jk_{yln}y}\right) \qquad (4)$$

where A^+_{ln} and A^-_{ln} are the mode amplitudes for the $(l,n)^{\text{th}}$ mode in section A and k_{yln} are the y-directed wavenumbers.

For convenience in the application of the boundary conditions, the fields in section D are separated into two parts, which are designated the primary and secondary fields. The y-dependencies Y^D_P of the primary fields consist of plane waves leaving the source in the $\pm y$-direction, i.e.,

$$Y^D_P \sim \begin{cases} \sum_{l,n} D^-_{Pln}e^{jk_{yln}(y-y')} & y < y' \\ \sum_{l,n} D^+_{Pln}e^{-jk_{yln}(y-y')} & y > y' \end{cases} \qquad (5)$$

The boundary conditions at the source ($y = y'$) are satisfied by the primary fields, and the primary field mode amplitudes $D^\pm_{Pln}$ are thereby explicitly determined. The y-dependencies Y^D_S of the secondary fields satisfy the homogeneous wave equation in all regions and consist of plane waves traveling in both directions, i.e., equation 4 with mode amplitudes D^+_{Sln} and D^-_{Sln}. The boundary conditions at $y = 0, b_1, b_2, b_3, b$ are used to generate two equations from which D^+_{Sln} and D^-_{Sln} are determined.

Mode-matching allows the boundary conditions at the section interfaces to be satisfied. The fields at $y = b_3$ are related to the fields at $y = 0$ by means of scattering matrices (which are numerically stable, unlike transmission matrices). The scattering matrix $S^{(3)}$ for the interface at $y = b_3$ is defined by

$$\begin{bmatrix} C^- \\ D^+_P + D^+_S \end{bmatrix} = \left[S^{(3)}\right]\begin{bmatrix} C^+ \\ D^-_P + D^-_S \end{bmatrix} \qquad (6)$$

where C^-, C^+, D^-_P, D^+_P, D^-_S, and D^+_S are all column vectors of the form $C^- = [C^-_{10}\ C^-_{20}\ \ldots\ C^-_{ln}\ \ldots]^T$. Similar equations exist which define the scattering matrices at the interfaces $y = b_1, b_2$. Reflection coefficient matrices $\Gamma^{(1)}$, $\Gamma^{(2)}$, and $\Gamma^{(3)}$ are defined by

$$B^+ = \left[\Gamma^{(1)}\right]B^- \qquad (7)$$

$$C^+ = \left[\Gamma^{(2)}\right]C^- \qquad (8)$$

$$D^+_S = \left[\Gamma^{(3)}\right](D^-_P + D^-_S) \qquad (9)$$

Application of the boundary conditions at $y = 0$ and manipulation of the scattering matrix equations allow $A^\pm$, $B^\pm$ and $C^\pm$ to be eliminated; hence the reflection coefficient matrices are

$$\Gamma^{(j)} = S^{(j)}_{22} + S^{(j)}_{21}\left(-S^{(j)}_{11} + \left(L^{(j)}\Gamma^{(j-1)}L^{(j)}\right)^{-1}\right)^{-1}S^{(j)}_{12} \qquad (10)$$

where $j = 1,2,3$; $L^{(j)} = \mathrm{diag}\{e^{-jk_{yln}(b_j - b_{j-1})}\}$; $\Gamma^{(0)} = -I$; and I is the identity matrix.

The boundary conditions at the conducting wall $y = b$ and manipulation of the matrix equations give an expression for the section D secondary field mode amplitudes D^-_S in terms of $D^\pm_P$. D^+_S is then determined from equations 9–10.

Given the x-, y- and z-dependencies of the fields generated by a point source, the components of the Green's function are known and the integral equation is solved with

the method of moments. The current is assumed to be z-directed. The transverse (i.e., x) variation of the current may be described with appropriate basis functions, such as an entire domain Maxwellian basis function which satisfies the edge condition, or pulses, which are necessary when the conductor does not have uniform width along the longitudinal direction (as in Figure 1). The longitudinal (i.e., z) variation of the current is described with piecewise-sinusoidal basis functions. When the current is expanded with these basis functions and Galerkin's method is applied, the integral equation yields a matrix equation for the unknown current coefficients I:

$$[V] = [Z][I] \tag{11}$$

The discontinuity is excited by a gap generator; hence $V = [00\cdots010\cdots]^T$ where the indexing of V is such that the '1' in the vector corresponds to the position of the gap generator on the conductor.

Characteristics of the discontinuity are extracted from the currents on the strip using either the standing-wave method [4] or the least squares Prony's method [5]. The latter method is especially useful because only a short length of conductor is required (minimizing the discretization associated with the method of moments), and a current which consists of multiple frequency components may be easily separated into its individual constituents.

III. RESULTS

The software was developed on HP/Apollo workstations, and was based on the code for the two-dimensional version of the technique. For most of the results presented, excellence convergence was obtained with 140 TE_x and 140 TM_x modes, and 400 modes in the longitudinal direction. The verification of the two-dimensional code, which includes all of the mode-matching portion of the technique, is discussed in [2]. The portion of the code which accounts for the extension to three-dimensional structures was verified by comparing with previously published characterizations of various shielded microstrip discontinuities.

In order to develop the expertise which is required to design and characterize a transition to a layered ridged dielectric waveguide, some simpler structures are first considered. The geometry of a microstrip on a dielectric ridge with an open end discontinuity is given in Figure 3, and samples of the characterization of this structure are displayed in Figures 4 and 5.

The first plot shows $\angle S_{11}$ as a function of frequency for various ridge widths d when substrate height h_1 and ridge height h_2 are constant. The difference in $\angle S_{11}$ between the case when the conductor covers the entire ridge ($d = 100\mu$m) and the case when the ridge is very wide (i.e., microstrip) is only 2-4°. The difference between the case when the ridge width is three times the width of the conductor ($d = 300\mu$m) and the microstrip case is insignificant.

The second plot shows $\angle S_{11}$ as a function of ridge height

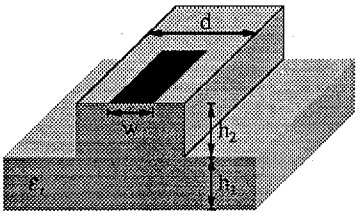

Figure 3: Conducting strip centered on a dielectric ridge. The ridge is centered in the cavity. $w = 100\mu$m; $\epsilon_r = 12.85$; cavity dimensions are $a = b = 1.2$mm and $c = 10.0$mm.

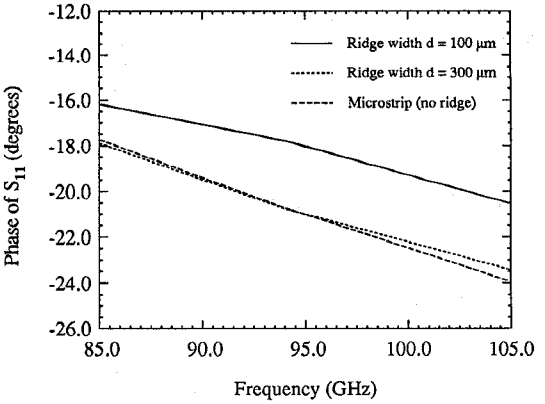

Figure 4: $\angle S_{11}$ vs. frequency for the strip-ridge structure of Figure 3 at ridge width $d = 100.0\mu$m and $d = 300.0\mu$m with $h_1 = h_2 = 50.0\mu$m. Also included is data for a microstrip ($h_2 = 0$).

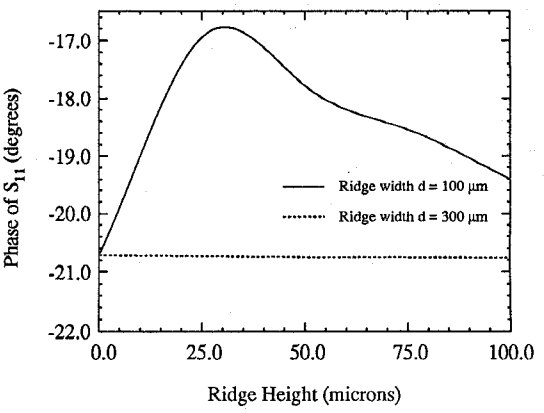

Figure 5: $\angle S_{11}$ vs. ridge height h_2, for the strip-ridge structure of Figure 3 at various values of ridge width d with frequency = 94 GHz and $h_1 + h_2$ constant at 100.0μm.

h_2 for various ridge widths d when frequency and total height ($h_1 + h_2$) are constant. When the ridge height is 0μm, all cases reduce to simple microstrip and $\angle S_{11}$ is the same for each curve. As the ridge height is changed from 0μm to 100μm (no substrate), a variation in $\angle S_{11}$ of only 4° occurs.

The data demonstrate that the behavior of the fields at the discontinuity is not strongly dependent on either ridge height or ridge width. A similar, more comprehensive study of complicated strip-ridge structures will yield necessary

information on how the alteration of ridge dimensions affects the performance of a transition to a layered ridged dielectric waveguide.

A first step in the characterization of an actual transition is the determination of a suitable strip-waveguide configuration. The propagation constants of two strip-waveguide test cases are displayed in Table 1. The "Microstrip Modes" are the propagating modes of the strip-ridge structures described in the Table; these results were obtained from the 3D IEMM technique and verified with the 2D IEMM software. The spatial distributions of the power density of the microstrip modes are similar to those of classical microstrip in that they extend from the top conductor down to the ground plane. The "Dielectric Waveguide Modes" are the propagation constants for the layered ridged dielectric waveguide without any conducting strips; these results were obtained from a mode-matching method. The power densities associated with the dielectric waveguide modes are distributed differently than those of the microstrip modes, in that they are concentrated in the lower layer of the ridge and do not penetrate extensively into the substrate or the upper layer (Figure 6).

These data suggest several considerations for the design of a transition. The wider strip-ridge supports two propagating modes, and one of these modes has a propagation constant which is extremely close to the propagation constant of the corresponding dielectric waveguide. The narrower strip-ridge supports only one propagating mode, and it is quite different from the dielectric waveguide mode. The former structure is possibly a better candidate for a transition, assuming that a criterion for a good transition is that the propagation constant of a mode in the strip-ridge structure match the propagation constant of the dielectric waveguide; further investigation will test this assertion. It is also possible that the transition could consist of a multi-mode strip-ridge structure feeding a unimodal dielectric waveguide; in general, then, optimization of the transition must be taken to mean minimization of the *total* reflected power contained by all the microstrip modes.

IV. CONCLUSION

With the ultimate goal being the characterization of a transition to a dielectric waveguide, the 3D IEMM technique has been presented. As a prelude to the characterization of an actual transition, the method was applied to some simple strip-ridge structures, and the data demonstrated that ridge height and width do not strongly affect the phase change associated with this particular type of open-end discontinuity. Initial results for two more complicated strip-ridge structures were also given, and one of the strip-ridge structures had a mode with a propagation constant similar to the propagation constant associated with the layered ridged waveguide alone. In order to realize the characterization of an actual transition, future results will include two-port structures, conductors with non-uniform widths along the longitudinal direction, and experimental results.

Substrate	GaAs $\epsilon_r = 12.85$	
Substrate Hgt.	17.1μm	
Lower Layer in Ridge	AlGaAs $\epsilon_r = 10.0$	
Lower Layer Hgt.	22.7μm	
Upper Layer in Ridge	GaAs $\epsilon_r = 12.85$	
Upper Layer Hgt.	58.2μm	
Ridge Width	100μm	40μm
Conductor Width	50μm	35μm
β—Microstrip Modes	$3.173k_o$ $1.598k_o$	$2.335k_o$
β—Dielectric W.G. Modes	$1.788k_o$	$1.218k_o$

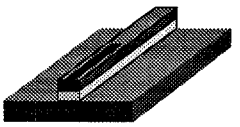

Table 1: Comparison of two strip-waveguide structures at 470 GHz. The layered ridged dielectric waveguide has a cross-section as described in Figure 2, and the strip is centered on the ridge.

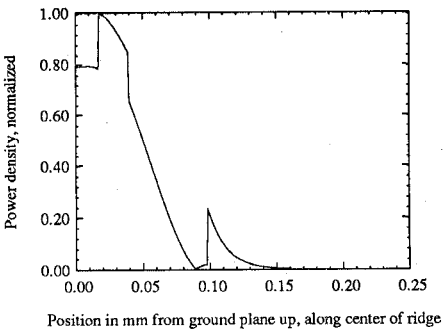

Figure 6: Power density of the propagating mode in the dielectric waveguide described in Table 1.

V. ACKNOWLEDGMENT

The authors are grateful to Mr. Nihad Dib for his contributions toward the successful application of Prony's method in this work.

This work was supported by the NASA Center for Space Terahertz Technology at the University of Michigan, and by the Army Research Office under Contract no. DAAL03-91-G-0116.

VI. REFERENCES

[1] A. G. Engel, Jr. and P. B. Katehi, "Low-loss monolithic transmission lines for submillimeter and terahertz frequency applications," *IEEE Trans. Microwave Theory Tech.*, vol. MTT-39, pp. 1847–1854, Nov. 1991.

[2] A. G. Engel, Jr. and P. B. Katehi, "Analysis of microstrip on and near dielectric ridges Using an integral equation-mode matching technique," *1991 IEEE MTT-S Int. Microwave Symp.*, vol. 1, no. D-4, pp. 135–138.

[3] F. E. Gardiol, "Higher-order modes in dielectrically loaded rectangular waveguides," *IEEE Trans. Microwave Theory Tech.*, vol. MTT-16, pp. 919–924, Nov. 1968.

[4] W. P. Harokopus, Jr., and P. B. Katehi, "Characterization of microstrip discontinuities on multilayer dielectric substrates including radiation losses," *IEEE Trans. Microwave Theory Tech.*, vol. MTT-37, pp. 2058–2066, Dec. 1989.

[5] S. L. Marple, *Digital Spectral Analysis with Applications.* Englewood Cliffs NJ: Prentice-Hall, Inc., 1987.